Magnetically driven drug delivery systems improving targeted immunotherapy for colon-rectal cancer

Renata Grifantini[1,3], Monia Taranta[2], Lisa Gherardini[2], Ilaria Naldi[2], Matteo Parri[3], Alberto Grandi[3], Ambra Giannetti[4], Sara Tombelli[4], Gioia Lucarini[5], Leonardo Ricotti[5], Susanna Campagnoli[3], Elisa De Camilli[6], Gualtiero Pelosi[2], Francesco Baldini[4], Arianna Menciassi[5], GiuseppeViale[6,7] Piero Pileri[3], and Caterina Cinti[2*].

1. *National Institute of Molecular Genetics (INGM), Milan, Italy*
2. Institute of Clinical Physiology, Experimental Oncology Unit, National Research Council (CNR) of Italy, Siena, Italy
3. Externautics Srl, Siena, Italy
4. Institute of Applied Physics, National Research Council (CNR) of Italy, Florence, Italy
5. The BioRobotics Institute, Scuola Superiore Sant'Anna, Pisa, Italy
6. European Institute of Oncology (IEO), Milan, Italy
7. Department of Oncology and hemato-oncology, University of Milan, Italy

*Corresponding author:
Caterina Cinti

Abstract

Colorectal cancer (CRC) is one of the major causes of cancer-associated mortality worldwide. The currently approved therapeutic agents show a rather limited efficacy. We have recently demonstrated that the atypical cadherin FAT1 is a specific marker of CRC and that the FAT1-specific monoclonal antibody mAb198.3 may offer new therapeutic opportunities for CRC, being efficiently internalized by cancer cells and reducing cancer growth in colon cancer xenograft models.

In this study we explored the therapeutic efficacy of mAb198.3 using two drug delivery systems (DDS) for improving the targeted treatment of CRC. The mAb198.3 was either directly bound to super-paramagnetic nanoparticles (spmNPs) or embedded into human erythrocyte-based magnetized carriers, named Erythro-Magneto-Hemagglutinin Virosomes (EMHVs) to produce two different novel mAb198.3 formulations. Both DDS were endowed with magnetic properties and were anchored in the target tumor site by means of an external permanent magnet. The antibody loading efficiency of these two magnetically driven drug delivery systems and the overall therapeutic efficacy of these two formulations were assessed both *in vitro* and in a proof-of-concept *in vivo* study.

We demonstrated that mAb198.3 bound to spmNPs or embedded into EMHVs was very effective in targeting FAT1-positive colon cancer cells *in vitro* and accumulating in the tumor mass *in vivo*. Although both in vivo administered mAb198.3 formulations have approximately 200 lower antibody doses needed, these showed to achieve a relevant therapeutic effect, thus reducing cancer growth more efficiently. respect to the naked antibody. These results indicate that the two proposed magnetically driven drug delivery systems have a considerable potential as platforms to improve bioavailability and pharmacodynamics of anti-FAT mAb198.3 and raise new opportunities for a targeted therapy of CRC.

Introduction

Colorectal cancer (CRC) is the fourth leading cause of cancer-related mortality worldwide, accounting for over 600,000 deaths every year [1]. The life expectancy of CRC patients varies dramatically depending on the tumor stage. The 5-year survival is 90% in early stages and drops to approximately 10% once metastasis has occurred [2] Metastatic patients treated with chemotherapy based on 5-Fluoro-Uracil (FU) or Capecitabine have a mean survival of approximately 12 months. Combination of chemotherapy with other approved targeted therapeutic agents increases the overall survival of only few months. Cetuximab and Panitumumab monoclonal antibodies (mAbs) are used to treat advanced CRC patients affected by tumors that over-express Epidermal Growth Factor Receptor (EGFR); they represent approximately 65-75% of all CRC patients [3]. The use of the mentioned drugs allows an overall survival benefit of approximately 5 months when used in combination with chemotherapy [4]. Moreover, CRC with mutations in V-Ki-ras2 Kirsten rat sarcoma viral oncogene homolog (*KRAS*) and v-Raf murine sarcoma viral oncogene homolog B (*BRAF*) are almost always resistant to treatment with the anti-EGFR antibodies [4]. Overall, the currently approved therapeutic regimens show a rather limited efficacy. Therefore, the development of other monoclonal antibodies towards CRC-associated targets is essential to improve life expectancy of CRC patients.

Grifantini R. and co-workers recently discovered a murine monoclonal antibody (mAb198.3) directed against *FAT1* that specifically recognizes CRC cells in human tissues, regardless of tumor stage and grade and also in the presence of *KRAS* and *BRAF* mutations [5]. The mAb198.3 binds to the surface of different FAT1-positive CRC cells and, upon binding, it is efficiently internalized exerting anti-tumor activity in xenograft mouse models of HCT15 and HT29 colon cancers [5]. It was recently demonstrated that such antibody can be used to selectively target CRC tumor mass when linked to anionic gold (AuCOOH) nanoparticles (NPs) [6] or to multifunctional nanoparticles based on SiO2@AuNP carrying three different anti-tumor drugs [7].

In this study, we further investigated the therapeutic potential of mAb198.3 by coupling it with two drug delivery systems (DDS) endowed with magnetic properties. The first system was based on superparamagnetic iron oxide nanoparticles (spmNPs) bound to the antibody; the second system was based on engineered human erythrocytes (Erythro-Magneto-Hemagglutinin Virosomes, EMHVs) embedding spmNPs and the antibody.

spmNPs are raising an increasing interest as contrast media for biomedical imaging [8] as well as for building innovative therapeutic tools, in particular for loco-regional ablative treatments [9] and magnetically-driven drug delivery [10]. The future of therapeutic applications of spmNPs would strongly benefit from an improvement in their capability to reach the selected target, in particular

beyond the intravascular space. Besides the functionalization of spmNPs with *ad hoc* bioactive molecules, external static magnetic fields are intriguing means to remotely influence the bio-distribution and concentration of spmNPs to a specific anatomical region or portion of a tissue, thus reducing the overall concentration of spmNPs administered to the body [11]. An efficient anchoring, indeed, would significantly improve the bioavailability of drugs linked to spmNPs at the target area, with a concomitant reduction of therapeutic drug doses. Notwithstanding their advantages, nanoparticles-based delivery systems may have different factors limiting their clinical application including their limited drug carrying capacity, *in vivo* circulation instability and the possibility of altering the drug action [12,13].

In the last years, cell-based carriers including leukocytes, hepatocytes and erythrocytes have been suggested as possible vehicles for therapeutic compounds [14]. In particular, the use of erythrocytes has gained remarkable interest to deliver various therapeutic agents and shows numerous advantages for several clinical applications. This kind of carriers constitutes an intriguing opportunity, especially for compounds that are expensive to synthesize, featured by a reduced half-life, which are systemically toxic or are rapidly inactivated *in vivo*, following administration [15]. Moreover, erythrocyte-based DDS have the ability to protect the loaded drug from degradation, can greatly reduce the possibility of acquiring a severe immunologic reaction when autologous erythrocytes are used and can act as bioreactors transforming the pro-drug in drug, due to their stable metabolic/enzymatic system [16]. Consequently, they can also reduce possible cytotoxic effects of the carried compounds [17] and can improve their pharmacokinetics and pharmacodynamics. In addition, erythrocytes can be magnetized, by entrapping spmNPs within them, thus making such DDS responsive to an external magnetic field [18]. This additional feature has the potential to increase targeting efficiency and to reduce potential off-site effects of the therapeutic compound.

In this paper we characterize and compare, in terms of therapeutic efficacy against CRC, the two above-mentioned DDS, based on spmNPs and EMHVs. Both of them were bound to or embedded mAb198.3 and both were subjected to magnetic targeting, thanks to the application of a static magnetic field. The results obtained with these two DDS are compared with the ones obtained with the naked mAb198.3, quantifying how much delivery systems contribute to increase the antibody bioavailability/pharmacodynamics and demonstrating their overall potential as tools for CRC therapy.

Material and Methods

Reagents and cell cultures.

Unless specified, all reagents were obtained from Sigma-Aldrich (Milan, Italy). mAb198.3 was

selected against the recombinant FAT1 region (aa 723-1352), using the hybridoma technology [19], as described in [5]. HCT15 cells were purchased by ATCC and cultured under recommended conditions.

Immuno-histochemical (IHC) analysis

For IHC analysis of primary and metastatic human tumors, formalin-fixed, paraffin-embedded (FFPE) tissue blocks of CRC resections from 5 primary CRC and 5 liver metastasis from colon cancer, isolated from the same patients (five patients in total), were retrieved from the archives of the European Institute of Oncology. CRC and normal samples were arrayed in parallel on the same tissue microarray slides and analyzed simultaneously. IHC slides were prepared in a conventional way and stained with the anti-FAT1 mAb198.3. Slides were screened semi-quantitatively for the percentage and the intensity of the signal for FAT1 [5]. Negative control samples were prepared by using an irrelevant isotype control antibody and/or by omitting the primary antibody. IHC staining and analysis were performed as previously described [5,20].

For IHC analysis of HCT15 tumor cells from mice treated with the two mAb198.3 DDS, specimens of xenograft tumors explanted at the end of treatment from selected animals were embedded in formalin using a conventional protocol. Individual slides from FFPE specimens were incubated in a humid chamber overnight at 4°C with rabbit anti-human Ki67 mAb (clone SP6, Thermoscientific) at a dilution 1:100, mouse anti-FHA(filamentous hemagglutinin) mAb , Statens Serum Institute) at the dilution 1:50 and anti-Cytokeratin Purified Clone CAM5.2 (CE/IVD) raised against the colon carcinoma cell line HT29 (D.B.A Italia, Srl.). After 5 min washing with PBS Tween 20%, secondary biotinylated antibody (30 min) and Vectastain Elite ABC reagent (30 min) were applied. For detection, slides were incubated with peroxidase substrate solution (DAB), counterstained with standard Meyer Haematoxylin protocol (Sigma-Aldrich) and analysed under an Olympus BX43 light microscope interfaced to a video camera for digital acquisition (DP20 Olympus). Imaging analysis was carried out by using CellSens Dimension Olympus software. Semiquantitative analysis of Ki67 antibody staining within tumor area was carried out by averaging measurements of 5 microscopic fields for each of the 3 sample sections examined, digitized at 40x magnification by Olympus Cell Sens software, and presenting not less than 100 viable CRC cells: the percentage of number of positive dark brown cells on total number of observed cells was used as an index of anti-Ki67 binding.

Immobilization of the monoclonal antibodies onto the spmNPs

spmNPs were purchased from Micromod Partikeltechnologie GmbH (Germany). They consisted of cross-linked dextran iron oxide composite particles (by carrying NH_2 groups on the surface) with an

average diameter-size of 50 nm. 1-Ethyl-3-[3-dimethylaminopropyl] carbodiimide hydrochloride (EDC) and N-hydroxysuccinimide (NHS) were purchased from Pierce (Illinois, USA). Covalent immobilization of the anti-FAT1 mAb198.3 and an irrelevant IgG1 isotype control mAb (isomAb) onto the magnetic spmNPs was performed as follows. The spmNPs suspension (5 mg/ml) was sonicated for 1 min (Falc Instruments s.r.l., Italy) and spmNPs were collected by centrifugation (ALC International s.r.l., Italy) for 15 min at 14000 rpm. Then, the supernatant was removed. 50 µl of semi-dry spmNPs were re-suspended for 2 h with 300 µl of antibody containing 360 µg of antibody (stock at 1.2 mg/ml) in presence of a EDC/NHS mixture as active-crosslinking chemicals. The excess of non-immobilized antibodies was removed by 4 cycles of centrifugation (5 min at 14000 rpm), supernatant removal and re-suspension in PBS. In the resulting mAb198.3-spmNPs and isomAb-spmNPs the COOH groups of the antibodies were covalently bound to the NH_2 groups present onto the spmNPs. Preparations were stored at 4°C in the dark until use.

Semi-quantitative analysis of mAb198.3 formulations

A semi-quantitative estimation of the recovered spmNPs linked to antibodies (mAb198.3 and isomAb) was achieved through spectrophotometry (Perkin-Elmer, Milan, Italy), comparing the absorbance of the spmNPs with a calibration curve obtained from the absorbance of spmNPs at different concentrations. The analysis indicated a final concentration of 0.73 mg/ml of spmNPs for both mAb198.3-spmNPs and isomAb-spmNPs. To quantify the amount of antibodies linked to spmNPs, both mAb198.3 and isomAb were labelled to the IRDye 800CWNHS ester Near Infrared (NI) Dye (LI-COR biosciences) accordingly to manufacture protocol. A 24-well plate was set with serial dilution of mAb198.3-IRDye and isomAb-IRDye (0.0008-0.0125 µg/µl) and detected by the NI detector Odyssey (LI-COR). mAb198.3-IRDye-NPs dose concentration was measured off line through curve fitting (y=5E+0.9X-371127; R^2 =0.99). The concentration of both antibodies linked to spmNPs was 1.2 µg in 200µl of crosslinked-spmNPs solution**.**

Preparation and characterization of mAb198.3-loaded EMHVs (mAb198.3-EMHVs).

Human erythrocytes were prepared by gradient centrifugation at 400 g for 30 min and then washed twice in 1X PBS (1.37 M NaCl, 57 mM KCl, 54 mM Na_2HPO_4, 45 mM KH_2PO_4 pH 7.4). 2×10^9 erythrocytes were lysed in 250 µl lysis buffer 1 (10 mM TRIS-HCl, 0.1 mM EDTA, 1 mM $MgCl_2$ pH 7.2) for 60 min at 0°C. The isotonicity was then restored by adding 130 µl of resealing buffer (65 µl of 10X PBS pH 7.4 and 65 µl of 15 mM $MgCl_2$ pH 7.4), supplemented with 2 µg of FHA, 0.1 mg of 30 nm super-paramagnetic NPs (Nanocs Inc.,Boston USA) and a 5 µg of mAb198.3. The suspension was incubated for 45 min at 37°C under mild agitation to promote resealing and obtain engineered erythrocytes loaded with mAb198.3 and spmNPs. mAb198.3-EMHVs formulations were

then washed twice with 1X PBS by centrifugation at 8,000 g for 15 min at 4°C, re-suspended in 1X PBS and stored at 4°C until used. The amount of mAb198.3 loaded into $1x10^9$ EMHVs (mAb198.3-IRDye-EMHVs) in 200 µl of volume was measured by infrared detector Odyssey (LI-COR) comparing the mAb198.3-IRDye-EMHVs or isomAb-IRDye-EMHVs fluorescence with calibration curve (R=0.993) ranging from 0.0008 to 0.0125 µg/µl of free labelled antibodies. The mAb198.3-IRDye-EMHV and isomAb-IRDye-EMHV concentrations were measured off line through curve fitting (y=5E+0.9X-371127; R^2 =0.99). The amount of both mAb198.3 and isomAb antibodies carried by $1x10^9$ EMHVs was 1.95 µg.

Magnetic characterization of spmNPs and EMHVs

To estimate the magnetic force F_m acting on the DDS, thus to guarantee an efficient anchoring with the external permanent magnet, in the desired site, the volumetric magnetic susceptibility χ and magnetization M parameters were calculated for both DDS. Magnetization curves were obtained by a vibrating sample magnetometer (VSM, PPMS 6000, Quantum Design Ltd). Different independent samples were dehydrated and tested. For each EMHV sample, an initial volume of 500 µl, with 1 x 10^9 engineered erythrocytes was used while for each spmNPs sample, an initial volume of 50 µl, with a concentration of 5mg/ml was used. The magnetization curves were expressed as the magnetization M in emu/g at different magnetic field strengths H in Oe. χ was calculated by using the following equation:

$$\boldsymbol{\varkappa} = \frac{\mathbf{M}}{\mathbf{H}}\boldsymbol{\rho} \qquad (1)$$

where ρ is the mean sample density of mAb198.3-spmNPs and mAb198.3-EMHVs formulations.

To estimate the magnetic force F_m allowing the DDS anchoring at the target site in presence of a known magnetic field ($\vec{H}$) produced by the external magnet, the following equation was used:

$$\vec{F}_m = V\vec{M}\cdot\nabla\mu_0\vec{H} = \mu_0 V \frac{3(\varkappa - \varkappa_0)}{[(\varkappa - \varkappa_0)+3]}(\vec{H}\cdot\vec{\nabla})\vec{H} \qquad (2)$$

where V is the DDS volume, μ_0 is the vacuum permeability and χ and χ_0 are the magnetic susceptibility of the samples, defined by equation 1, and the magnetic susceptibility of the vacuum, respectively [21].

To obtain an efficient magnetic anchoring of the proposed DDS, the constraint described by the following equation was respected:

$$\vec{F}_m + \vec{F}_D \geq 0 \quad (3)$$

where F_D is the drag force in the capillary that can be approximated by applying the Stokes law for a sphere in a laminar flow (both DDS can be considered a sphere) as follows [24]:

$$\vec{F}_D = -6\pi\omega r\vec{v} \quad (4)$$

where ω is the viscosity of the blood, r is the radius of the sphere that approximates the DDS and v is the DDS speed.

In order to respect the constraint described by equation (3), the magnetic field and the magnetic field gradient produced by the magnet (a N52 NdFeB cylinder with a diameter of 10 mm and a height of 6 mm) were estimated through Finite Element Model (FEM) simulations (Comsol Multiphysics 5.2a). In agreement with the anatomical constraints of the animal model, the magnet was placed at a distance of 2 mm from the target site. The FEM results were preliminary validated by an experimental assessment carried out by using a Hall sensor (Magnetometer KOSHAVA 5, Wuntronic, GmbH).

In order to obtain an efficient anchoring of both systems, by elaborating the equations (2), (3) and (4), the following condition has to be respected for the magnetization M, expressed in A/m:

$$M \geq \frac{9\mu v}{2r^2\nabla B} \quad (5)$$

Flow Cytometry analysis of HCT15 cells treated with mAb198.3-spmNP

HCT15 cells (2 x10^4/well) were pelleted in 96 U-bottom microplates and incubated for 1 h at 4 °C with the appropriate dilutions of mAb198.3 or isomAb, linked to magnetic nanoparticles, as compared to the freely soluble mAbs. Cells were washed two times in PBS–5% FCS and incubated for 20 min with R-phycoerythrin (PE)-conjugated secondary antibody (Jackson ImmunoResearch, West Grove, PA, USA) at 4 °C. Cells were analyzed by a FACS-Canto-II flow cytometer (BD Biosciences, San Jose, CA, USA) and data were analyzed with the FlowJo (Ashland, OR, USA) software.

Confocal Laser scanning microscopy (CSLM) imaging of mAb198.3-EMHVs.

For Confocal Laser scanning microscopy (CSLM) imaging of mAb198.3-EMHVs samples, a batch of EMHV was produced including auto-fluorescent rodamine-conjugated magnetic nanoparticles and antibodies conjugated with green fluorescence Alexa-fluor488, which were labelled using the Alexa Fluor™ 488 Antibody Labeling Kit (Thermo Fisher). Double labelled mAb-EMHVs were fixed on a coverslip and analyzed by CSLM imaging, to confirm the co-inclusion of antibodies and magnetic nanoparticles. An Argon laser with an excitation wavelength of 488 nm and emission at 519 nm was used for detecting antibodies, while excitation at 514 nm and emission at 575 nm were used for detection of rhodamine-conjugated nanoparticles.

Tumor xenograft animal model and treatments

Model setting. HCT15 human colon carcinoma cells (5x10^6) were injected subcutaneously into the right flank of nude athymic mice (Harlan laboratories, 8 mice/group). Tumor growth was monitored

measuring with a caliper the greatest longitudinal diameter (length) and the greatest transverse diameter (width). Tumor volumes were estimated by the modified ellipsoidal formula: tumor volume = 1/2(length x width^2). Treatment started when tumor reached more or less 100 mm^3. Before each injection, tumor volumes (volume$_1$) were measured and compared to the corresponding initial volumes (volume$_0$), in order to normalize the data (X = 100 x volume$_1$/volume$_0$).

Treatments. Mice were treated i.v. with repeated doses of 300 μg in 200 μl of PBS of either free mAb198.3 and free isomAb. They were compared with mice treated with 1.2 μg/dose of mAb198.3 or isomAb linked to spmNPs, or with 1x10^9 EMHVs containing 1.95 μg mAb198.3 both in the presence of external static magnetic field generated by a N52 NdFeB magnet (diameter of 10 mm and height of 6 mm) (Supermagnete, Italy). The control group was treated with saline solution. For all treatments, injections were performed biweekly for three weeks.

Mice bearing tumors bigger than 1500 mm^3 were sacrificed. The care and use of animals strictly applied European and National Regulation for the Protection of Vertebrate Animals used for Experimental and other Scientific Purposes in force and approved by the local Animal Welfare Body (AWB) and by the Italian Ministry of Health (approved experimental protocol 030314).

Ethics Statements

Human red blood cells were obtained from transfusion bags collected from anonymous healthy voluntary donors, which have given their written informed consent in accordance with the Italian Government law. The approval from an institutional review board (ethics committee) was not needed, since neither direct human participation nor involvement of human studies have been foreseen in this work. The Azienda Ospedaliera Universitaria Senese (AOUS) provided the blood samples. Concerning IHC analysis, it was conducted on archived CRC samples from five patients that had given their informed consent for using the remaining tissue after histopathological diagnosis for non-interventional, observational research studies.

The preclinical studies were carried out in strict accordance with the recommendations in the Guide for the Care and Use of Laboratory Animals of the International guidelines on handling of laboratory animals (R4 guideline of NIH and European Commission recommendations). The protocol for Animal Experiments was approved by the Ethics Committees of the Toscana Life Sciences and the Istituto Superiore di Sanità (ISS) on behalf of Italian Minister of Health (Permission Number: # CNR-270111 exp1/prot1). Animal wellbeing was monitored accordingly to the indications of Langford et al [22].

Statistical analysis of in vivo experiments

To evaluate mAb 198.3 enrichment at tumor sides in the groups of injected animals versus controls, a one-way ANOVA was performed. To validate the treatment effects over the time of administration, a two-ways repeated measure analysis ANOVA was applied. Statistical significance threshold was set at a P value < 0,05.

Near Infrared imaging of mAb198.3 localization (ODYSSEY)

Infrared Imaging was used to evaluate the localization of 300μg mAb198.3 labelled with IRDye moiety. 300μg of mAb198.3-IRDye was administered by intra-caudal (i.v.) or intra-tumor (i.t.) injections. Antibody enrichment was verified by total body scanning using the Near Infrared (NI) Odyssey instrument (LI-COR). Measurements were performed off line using Volocity, (PerkinElmer) calculating pixel signals of a region of interest (channel 800nm) in correspondence of the tumor mass in i.t and i.v treated and control animals and expressed as arbitrary fluorescence unit (a.f.u). Two-way ANOVA statistical analysis was performed.

High-resolution ultrasound and Power Doppler Modes of blood flow in xenografts

An ultrasound 2100 VEVO system (Visualsonics) was used to qualitatively describe the blood flow variation during injection of the drug delivery bolus at the tumor mass in xenografts.

Animals were anesthetized by Isofluorane (IsoFlo, Abbott induction rate 3.5% and maintenance 2-1,5%) and placed on a mouse pod to maintain body temperature at 37° C, under an oxygen flux (1L/min of O2 95%). The i.v. injection lasted about 10 s and the localized signal was recorded for the whole duration of the injection. Video frames were selected to visualize the salient phases of the injected treatment flux.

Results

mAb198.3 recognizes CRC at different progression stage with similar efficiency

An important property of any new potential drug for CRC is the ability to target advanced states of the disease. In a recent study the authors showed that anti-FAT1 mAb198.3 specifically recognizes its target FAT1 antigen in both primary and metastatic CRC with similar efficiency [5]. Here we further investigated the mAb198.3 ability to recognize CRC at different progression stages by analysing formalin-fixed paraffin-embedded (FFPE) CRC samples derived from surgical resections of five local primary lesions and five matched liver metastasis isolated from the same patients (five patients, in total) after staining with mAb198.3. All CRC samples showed a clear membranous antibody staining that extended in part to the cytoplasm, with similar intensity and homogeneity both

in local and distal metastases, with only a marginal background staining in normal hepatocytes surrounding the metastatic lesions and in normal colon mucosa (**Figure 1**).

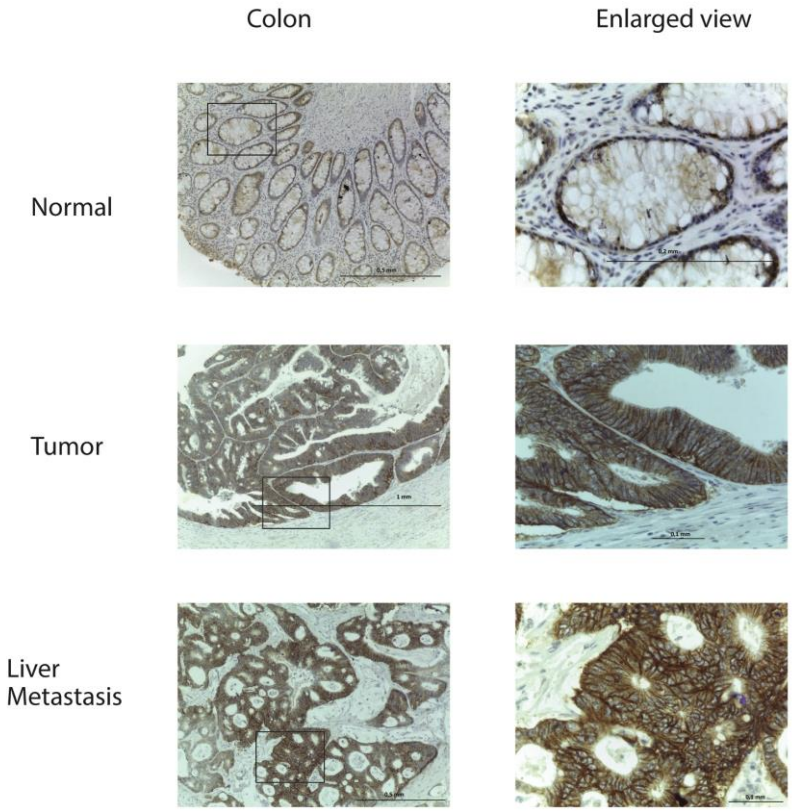

Figure 1. **mAb198.3 detects FAT1 with similar efficiency in primary and metastatic CRC**. FFPE samples derived from surgical resections of local primary CRC lesions, matched liver metastasis and normal control samples isolated from the same patients were stained with mAb198.3. All CRC samples showed a strong membranous antibody staining of cancer cells that extended in part to the cytoplasm, with similar intensity and homogeneity both in local sites and distal liver metastasis**.** Epithelial cells of corresponding normal samples showed only a marginal background staining.

anti-FAT1 mAb198.3 linked to spmNPs efficiently binds colon cancer cells

With the purpose to improve the pharmacokinetics of mAb198.3, we used a magnetically driven DDS based on superparamagnetic nanoparticles (spmNPs). To this aim we assessed the ability of mAb198.3 to maintain its specificity and tumor targeting activity when delivered in this formulation. mAb198.3 and its isotype-matched antigen-unrelated control (isomAb) were cross-linked to spmNP. A final concentration of 1.2 μg in 200 μl of spmNP suspension was achieved for either of the two antibodies. The mAb198.3-spmNP formulation was compared to free mAb198.3 in terms of ability

to bind the FAT1-positive HCT15 colon cancer cell line, by using flow cytometry. As shown in **Figure 2**, mAb198.3–spmNP efficiently bound HCT15 colon cancer cells, similarly to the free mAb198.3 (right panel). This demonstrated that the immobilization of mAb198.3 to spmNP did not influence the antibody ability to recognize FAT1 on the cell surface.

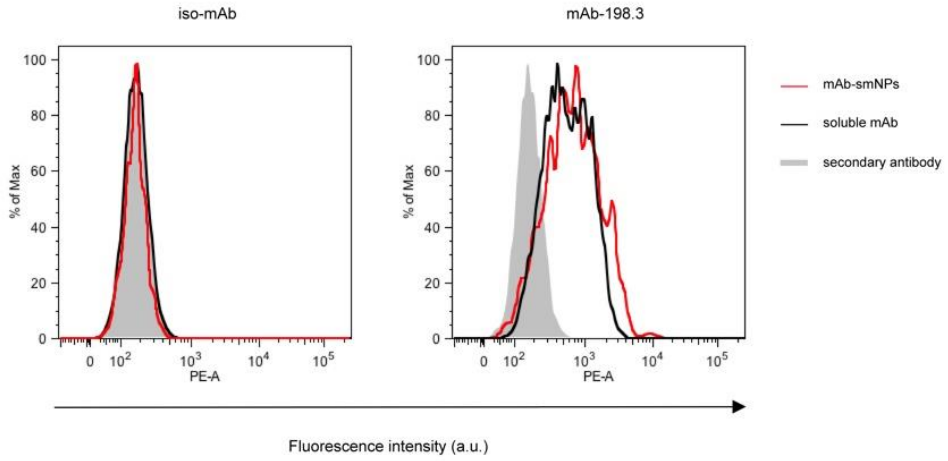

Figure 2. **mAb198.3 linked to spmNPs maintains its ability to bind colon cancer cells**. HCT15 tumor cells were surface stained with iso-mAb (left panel) or mAb-198.3 (right panel) either in soluble form (black line) or linked to smNPs form (red line) followed by PE-labeled secondary antibody. Cells labeled only with secondary antibody are shown in the grey solid peak.

EMHVs efficiently co-entrap both mAb198.3 and spmNP

In addition to spmNPs, we investigated the opportunity to use an additional magnetically driven DDS, based on engineered erythrocytes (EMHVs) as carriers of mAb198.3, for a targeted delivery to cancer lesions. Such system has the potential to bring the antibody in the tumor area and to deliver it into the intracellular compartment of cancer cells exploiting the hemagglutinin-based membrane fusion mechanism, thus improving the overall antibody bioavailability and pharmacodynamics properties. We thus generated EMHV DDS[23] containing both mAb198.3 and spmNPs. The mAb-198.3-EMHV formulation was characterized by Confocal Laser Scanning microscopy, confirming that an efficient co-inclusion of both mAb198.3 (green, **Figure 3a**) and spmNPs (red, **Figure 3b**) in almost all EMHVs were double labelled (yellow, **Figure 3d**) is visible. The amount of mAb198.3 antibody entrapped into 1 x 10^9 EMHVs, estimated by near-infrared semi-quantitative analysis, was 1.95 μg.

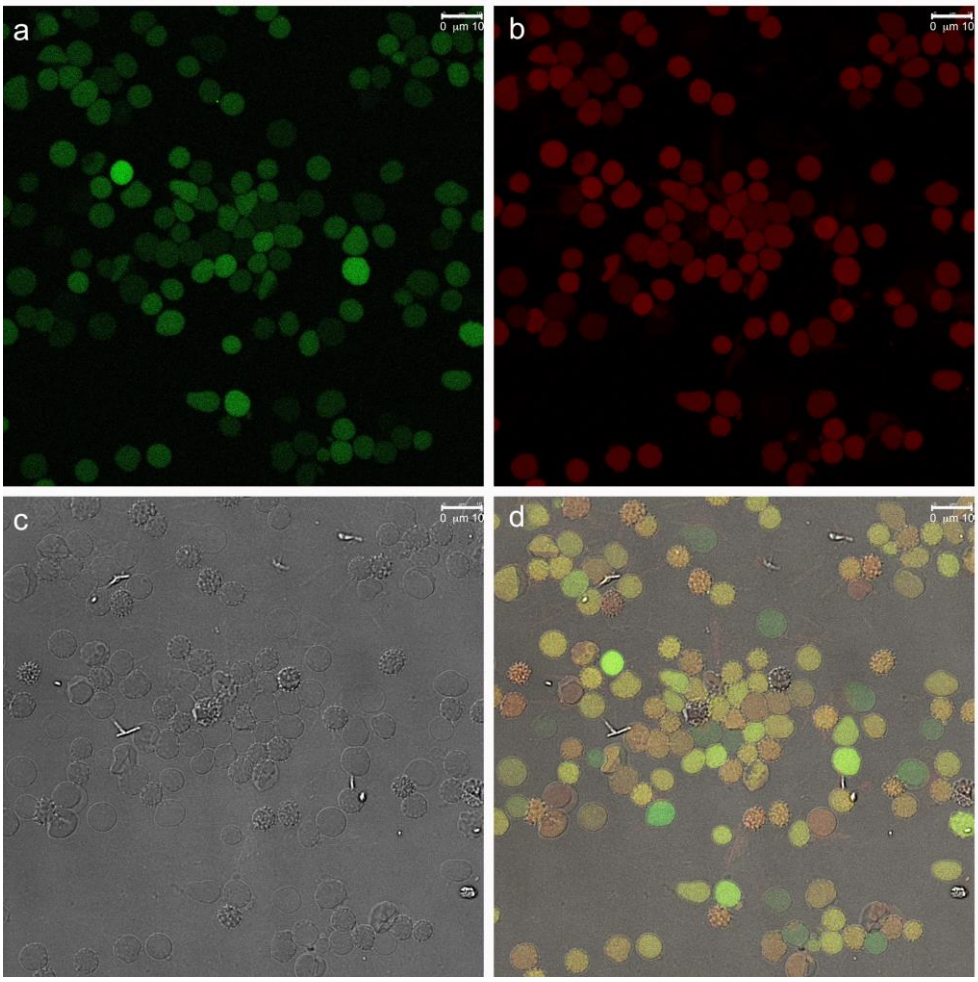

Figure 3: **Confocal laser scanning microscopy images of EMHVs loaded with mAb198.3 and spmNPs.**
EMVHs were prepared in the presence of Alexa-488-labeled antibodies and rhodamine-conjugated nanoparticles and the co-entrapment efficiency was assessed by confocal microscopy. (a) EMHVs Green fluorescence of Alexa-488-labeled antibodies. (b) Red fluorescence of rhodamine-conjugated nanoparticles. (c) Bright-field image of EMHVs. (d) Merged image.

Magnetic characterization and attraction of spmNPs and EMHVs The proposed DDS (i.e. spmNPs and EMHVs) were endowed with magnetic properties and could be thus anchored at a target site by exploiting magnetic fields. Magnetization depends on volume/mass and on the type of magnetic particles entrapped inside (i.e. in EMHV) or linked to antibody (i.e. in spmNPs). Therefore a magnetic characterization was performed to evaluate if the same external magnetic fields can be used for accumulation onto the target site for both DDS. The results of FEM simulations, describing the magnetic field and the magnetic field gradient generated by the permanent magnet are reported in **Figure 4**. A magnetic field of 0.1 T and a magnetic field gradient of 4 Gauss/m were produced by the magnet at a distance of 2 mm from the magnet surface. Such distance corresponded to the average tumor depth in the animal tests described in the following, thus it represented a realistic distance value between the skin (and magnet) surface and the target site for the DDS.

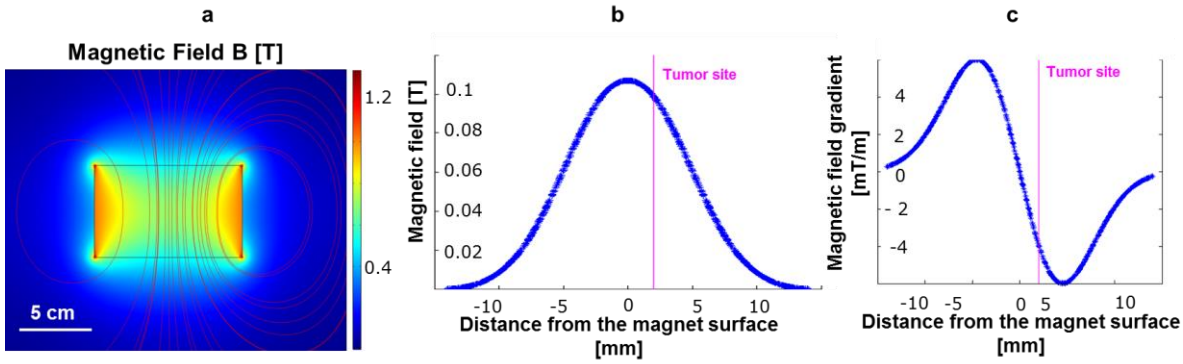

Figure 4: Magnetic field and magnetic field gradient produced by the external permanent magnet. (a) Magnetic field map obtained by FEM simulations: the color bar indicates the magnetic field expressed in T. Magnetic field (b) and magnetic field gradient (c) calculated along the magnet axis. The violet line identifies the distance of the tumor site from the skin (and magnet) surface, in agreement with the in vivo test conditions.

The results obtained from the DDS magnetic characterization are shown in Figure 5.

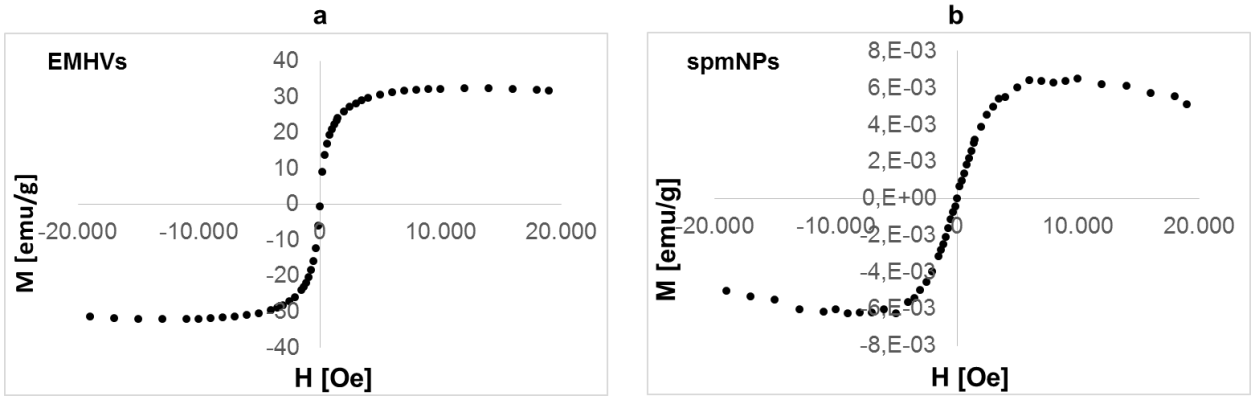

Figure 5: Representative magnetization curves for EMHVs (a) and spmNPs (b), obtained through a vibrating sample magnetometer. The M values are reported, for the two DDS.

By combining the results of Figure 4 and Figure 5, it was possible to check if the constraint expressed by equation (5) was respected. The following parameters were considered: a speed in the capillary (v) of 1 cm/s, a viscosity (ω) of 10^{-3} Pa·s and a EMHV and spmNPs density of respectively 5.3 x 10^4 and 1.4 x 10^3 Kg/m^3. By using such data and considering the results obtained, the minimum M value allowing the DDS to stop at the tumor site resulted $7 \cdot 10^5$ A/m for EMHV and 4.5 $\cdot 10^9$ A/m for spmNPs. As shown in Figure 5, both EMHVs and spmNPs showed higher M values (mean values of $1.9 \cdot 10^9$ A/m and 0.9 10^{11} A/m respectively for EMHVs and for spmNPs). Thus, both systems, in the described conditions, are subjected to a magnetic force that is able to contrast the physiological drag force, thus allowing an efficient anchoring at the target site.

mAb198.3 selectively localizes in cancer cells in vivo.

In previous authors' reports the ability of free mAb198.3 to specifically bind colon cancer cells in vivo, after subcutaneous intravenous injection (i.v) of the antibody in athymic mice subcutaneously engrafted with either HCT15 or HT29 cells, was demonstrated [5]. In this study, we further verified mAb198.3 specificity for colon cancer cells in athymic mice bearing subcutaneous HCT15 colon cancer xenograft injected with 300 μg IRDye-labelled antibody directly into the tumor (intra-tumor, i.t.) or with the same amount of antibody administered intra-venous (i.v.). These groups were compared with untreated mice receiving the saline solution (Controls, CT). The analysis of off-line pixel signal on NI-emitting area revealed a similar fluorescent signal (ONE WAY ANOVA: $P > 0.05$) in the i.t. (192.48 ± 23 a.f.u) or i.v (175.76 ± 35 a.f.u) injected animals (**Figure 6**) indicating that 91.3% of intravenous injected mAb198.3-IRDye remained maximally confined in the tumor area, with negligible spread in internal organs when compared to untreated animals. This result further confirmed mAb198.3 selectivity for colon cancer cells, with minimal off target interaction.

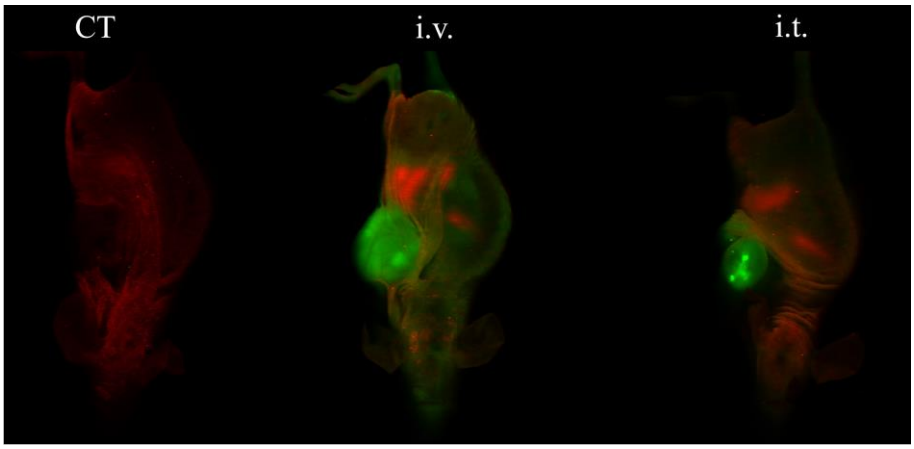

Figure 6. mAb198.3 selective localization at the tumor site, in vivo. Mice were injected with 300 μg of NI IRDye-labelled mAb198.3 either intravenous (i.v) and intra-tumoral (i.t). The distribution of i.v. (central panel) or i.t. (right panel) injected IRDye-labelled antibody was assessed by NI-Odyssey imaging. The IRDye signal (green) of i.v. and i.t. was compared to the level of the basal signal for untreated animals (CT) (left panel).

spmNP and EMHV DDSs improve the antitumor activity of mAb198.3 in a xenograft colon cancer mouse model

The mAb198.3 antitumor activity for colon cancer was evaluated *in vivo* in athymic mice bearing subcutaneous xenograft of approximately 100 mm^3, treated i.v. biweekly for three weeks with either naked mAb198.3 (300 μg /dose) or mAb198.3-spmNP (1.2 μg /dose) or mAb198.3-EMHVs ($1x\ 10^9$ EMHVs containing 1.95 μg mAb198.3/dose) and compared to mice treated with corresponding amounts of naked isomAb (300 μg /dose) or isomAb-spmNP (1.2 μg /dose) or saline solution (**Figure**

7). For all experimental groups, a N52 NdFeB permanent magnet with the same features of the one modeled in Figure 4 was placed on the mouse skin, in correspondence to the tumor site, immediately after antibody/DDS injection, and kept in position for 30 min.

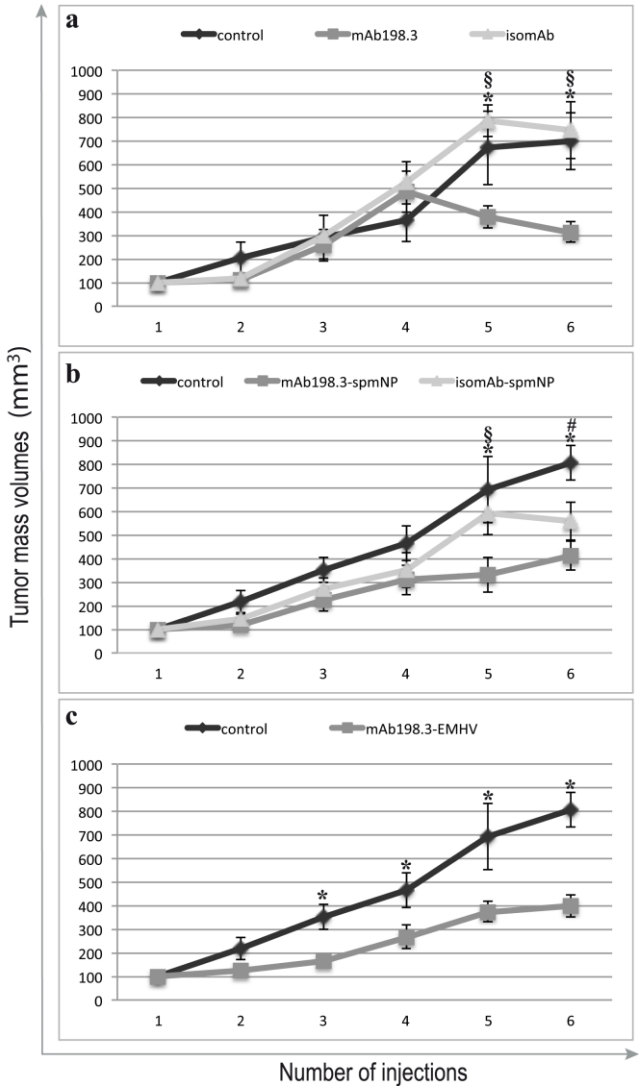

Figure 7. Therapeutic efficacy of mAb198.3-based treatments. Mice bearing subcutaneous HCT-15 xenografts were injected with mAb198.3, either as free molecules (300 μg/dose) or associated with spmNPs (1.2 μg /dose) or EMHVs (1.95 μg/dose). Tumor mass volume (y axis) is put in relation to the number of injections (x axis). The antitumor effect of (a) free mAb198.3 treatment with respect to both isomAb (§) and control (*) (two ways ANOVA RM $p<0.001$), (b) mAb198.3 linked to super-paramagnetic nanoparticles (mAb198.3-spmNPs) with respect to control (*) and isomAb-spmNP (§) (two ways ANOVA RM $p< 0.003$) and (c) mAb198.3-EMHVs with respect to controls (*) (two ways ANOVA RM $p<0.001$), are shown.

As shown in **Figure 7a**, free mAb198.3 (300 μg/dose) induced a significant anti-tumor effect, expressed as normalized tumor mass volume (y axis), starting from the 5^{th} injection (x axis) with respect both to equivalent free isomAb and control (two ways ANOVA RM $p<0.001$).

Similarly, mAb198.3 linked to super-paramagnetic nanoparticles (mAb198.3-spmNP, 1.2 μg /dose) significantly reduced tumor growth starting from the 5th injection up to the 6th one, with respect to control and to isomAb-spmNP (Two Ways ANOVA RM $p< 0.003$) although mAb198.3-spmNP formulation employed an antibody dosage at least 300 fold lower than the free mAb198.3 treatment (**Figure 7b**). These results indicate an improvement in terms of pharmacodynamics of mAb 198.3 formulated with the magnetic nanoparticle carrier.

In correspondence to the 6th injection, the administration of isomAb-spmNPs caused a measurable inhibition of tumor growth with respect to control group that might be ascribed to an intrinsic NP toxicity on cancer cells, which was often observed after recurrent injections, due to their accumulation in the cancer area (**Figure 7b**).

Then, we explored the potential of EMHVs to drive mAb198.3 onto the tumor cells in order to enhance its bioavailability and pharmacodynamics properties. To this aim 1 x 10^9 EMHVs containing 1.95μg mAb198.3/dose were administered systemically and focused on the tumor xenograft by means of the permanent magnet. This mAb198.3-EMHV formulation induced a significant reduction in tumor growth as compared to the control group treated with saline solution (Two Ways ANOVAPM $p< 0.001$) (**Figure 7c**). Notably, tumor mass reduction appeared earlier **(**from the 3rd injection) in mAb198.3-EMHV treated animals with respect to free mAb198.3 and mAb198.3-spmNP ones**.** Thus, the conjugation with EMHVs resulted in a more effective treatment, at early time-points, in comparison with the other tested ones. At the 6th injection, the overall tumor volume for animals treated with mAb198.3-EMHV resulted almost equal to the one measured in mAb198.3-spmNP animals and slightly larger in comparison with the free mAb198.3 group. However, the amount of mAb198.3 loaded into the EMHV carriers was 300 fold lower than the freely administered dose. Thus, the therapeutic efficacy of such carrier can be considered very high.

The ability of mAb198.3-EMHVs to flow through the bloodstream and reach the tumor mass was monitored by imaging through Power Doppler Mode the area corresponding to the xenograft tumor mass. Erythrocytes are natural contrast agents for ultrasound detection and Power Doppler Mode imagining is an elective tool to visualize blood flow changes. As shown in **Figure 8**, the bolus flux induced a specific Doppler signal distinct from normal blood flow thus allowing selective monitoring of EMHV DDS delivering to the area corresponding to the tumor xenograft.

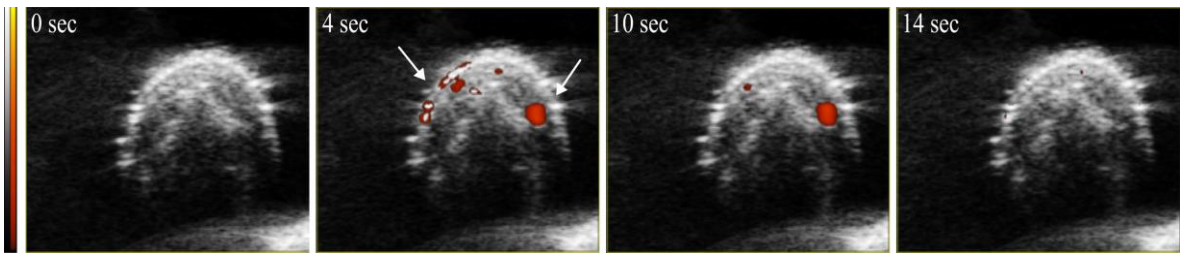

Figure 8: Power Doppler Mode imagining of the i.v. injected mAb198.3-EMHV reaching the xenograft tumor mass. The selected images show basal blood flux detected at 0 seconds (a), the pick of EMHV flux (red signal) reaching the mass at 4 seconds after IV injection (b, arrow), reduction of EMHV flux at about 10 second after injection (c) and return to basal conditions (d) of blood flux. The red bar indicates flux signal increment; the grey bar indicates the range of tissue ultrasonic density.

Upon mAb198.3-EMHV injection at 0 sec, we observed that the Doppler signal steadily grew from a basal signal and reached its pick at 4 sec highlighting tumor vascularization (**Figure 8a and b**), then it steadily reduced and reached back its basal level after 14 sec (**Figure 8c and d**).

Overall, both mAb delivery systems induced a tumor mass reduction similar in amplitude to that obtained with the free antibody treatment, albeit using a 2 log lower antibody dose, and the anti-cancer effect mediated by mAb198.3-EMHV appeared earlier than mAb198.3-spmNPs and the antibody alone.

IHC analysis of HCT15 tumors treated with mAb198.3 DDS

At the end of the experiments, HCT15 xenografts were explanted from animals for IHC staining with antibodies against the proliferation marker Ki67, the anti-pancytokeratine marker used for qualitative identification of normal cells and malignant cells of epithelial origin, and the FHA protein used to detect the presence of EMHVs (representative micrographs of selected FFPE samples are shown in **Figure 9**.

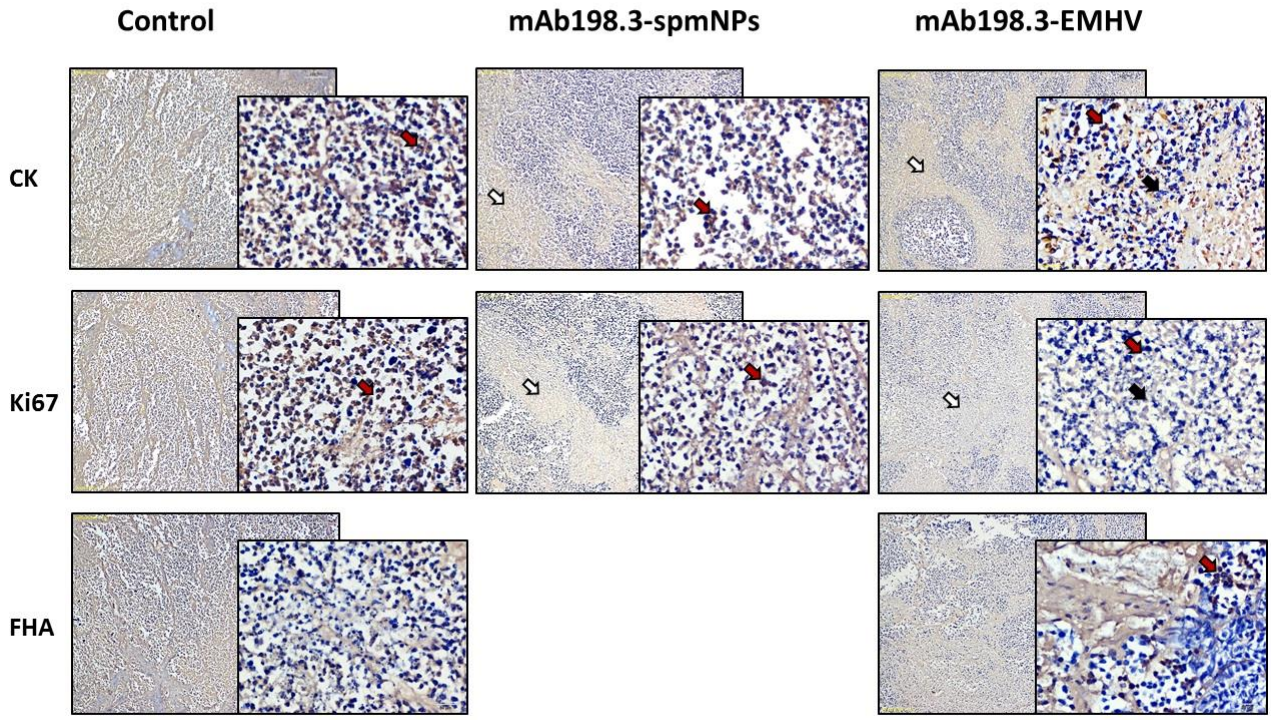

Figure 9. IHC analysis of explanted xenograft tumors. Immunodetection of panCytokeratin (CK), Ki67 and FHA in sample sections of untreated mice (control) and mAb198.3-spmNPsm and mAb198.3-EMHV treated mice. Low (10x original magnification) and high power (40x original magnification) micrographs (left and right micrograph respectively) are shown. From top to bottom: At low magnification, confluent areas of CRC necrosis are observed in treated cases, especially following mAb198.3-EMHV treatment (light arrows). At high magnification, anti-CK and anti-Ki67 positive stain (red arrows) of CRC cells (cytoplasm and nucleus respectively) is observed in untreated mice sections and at a markedly lower extent, in treated cases. Apoptotic bodies are present in several microscopic fields following mAb198.3-EMHV treatment (blue arrows). Anti- FHA staining is negative in untreated (Control) and positive (red arrows) in mAb198.3-EMHV treated mice sections.

A cytoplasmic cytokeratine staining and a nuclear Ki67 staining were detected in CRC cells in all sample sections of untreated animals (Control). Such positive staining was rarely observed in samples from mice treated with mAb198.3-spmNPsm and even less in mice treated with mAb198.3-EMHV, which showed extensive areas of necrosis and nuclear damage (pyknosis and apoptotic bodies).

The semi-quantitative Ki67 index was 40 ± 10% in untreated mice as compared to 15 ± 5 % and 3 ± 3 % immune-positive cells in sample sections of mAb198.3-spmNPsm and mAb198.3-EMHV treated mice. Anti-FHA positive cells were detected only in sample sections of mAb198.3-EMHV treated mice indicating the presence of EMHV carrier targeting HCT15 tumor cells.

DISCUSSION

Treatment of patients with advanced CRC still represents an unmet medical need. Intensive therapeutic protocols likely require multiple agents, such as chemotherapy agents, signalling inhibitors and mAbs, to interfere with disease progression and improve life expectancy. Therapies based on mAbs are particularly promising, thanks to their specificity for cancer cells and their antitumor activities through multiple mechanisms. At present, three mAbs (cetuximab, bevacizumab and panitumumab), directed towards molecules overexpressed on cancer cells like EGFR and VEGF, are routinely used for the treatment of colorectal cancer and many others are undergoing clinical trials [4]. Moreover, antibodies blocking CTLA-4 and PD-1/PD-L1 immune checkpoints have recently opened a new avenue for the treatment of colon cancer [25–27]. Despite the recent progress in the field, the fraction of oncologic patients that do not respond to the currently approved therapies is still high and there is an urgent need to identify and exploit novel targets to increase the tools available to provide an effective treatment for all CRC patients. To address this need, we recently reported that the proto-cadherin FAT1 antigen could represent a novel target for CRC therapy and we provided preclinical evidences of the therapeutic potential of the anti-FAT1 mAb198.3 as naked molecule [5].

In the first part of this study we further highlighted the potential application of mAb198.3 in CRC diagnosis. Interestingly we found that mAb198.3 specifically recognized CRC at different progression stages, being able to detect FAT1 both in local primary lesions and liver metastasis isolated from the same patients. The antibody showed a clear membranous staining in primary and metastatic human tumors that extended in part to the cytoplasm, both in local and distal lesions, with marginal background staining in normal hepatocytes surrounding the metastatic lesions and in normal colon mucosa. Moreover, we showed that the fluorescently labelled mAb198.3 had high tumor specificity and selectivity when injected i.v. in mice, suggesting that it could also have a high potential as molecular marker for clinical diagnostic imaging.

The therapeutic potential of mAb198.3 was also highlighted, by showing that its pharmacodynamic properties can be improved when delivered by innovative nanotechnology-based drug delivery systems (DDSs). Inorganic nanoparticles such as gold nanoparticles (AuNPs), iron oxide magnetic nanoparticles (MNPs), and quantum dots have been widely explored as a promising candidate for various biomedical applications including diagnostics (cell labelling, biosensing, *in vivo* imaging, bimodal magnetic-luminescent imaging) and therapeutics (local thermoablation and targeted delivery) due to their unique physicochemical properties [28]. AuNPs are mostly used as nano-biomaterials for *in vivo* imaging, due to their optical characteristics (strong absorption and scattering intensity), but also for target drug delivery when linked to specific biomacromolecules, owing to their excellent biocompatibility and low cytotoxicity [29]. We have previously shown that mAb198.3

linked to anionic gold AuNPs was an efficient tool for *in vivo* diagnostic imaging and targeting [6]. In addition, a multifunctional SiO2@AuNP drug delivery system was developed to sequentially release mAb198.3, Doxorubicin and siRNA at the tumor site [7].

Based on these encouraging results, in this study we further explored magnetic nanoparticles (MNPs) for mAb delivery. Currently, MNPs are customized for disease detection and treatment, particularly as contrast agents in diagnostic magnetic resonance imaging (MRI) as well as drug carriers in drug-targeted delivery systems and in hyperthermia treatment (treating tumors with heat). Because of their biocompatibility and magnetic properties, MNPs are a very attractive option as next generation drug carriers. The capability of MNPs to potentiality act as target drug delivery system strongly relies on external magnetic fields, which can remotely influence MNPs physiological bio-distribution, by directing and concentrating them to the desired pathological region. We have previously shown that it is possible to quantitatively detect spmNPs accumulation in vivo at low concentration and assess their tridimensional distribution in response to an external magnetic field and in relation to the local anatomy highlighted by PET/CT imaging [11]. In this study we demonstrated that spmNPs are more efficient than other NPs to reach target tissues without requiring *ad hoc* specific functionalization for the targeting. The sole physical magnetic field is sufficient to specifically drive this type of nanoparticles. This kind of targeted delivery allows a reduced drug dosage and improves the efficiency of linked drugs, which ultimately results in reduced adverse systemic and side effects to normal tissues. Although the potential benefits of MNPs are considerable, the low drug loading capability and the potential toxicity of MNPs generated by different surface coatings are the most sensitive parameters that should be improved in the future.

In this study we investigated two novel magnetically driven mAb198.3 formulations for FAT1 targeting in CRC.

In the first formulation, the mAb198.3 was directly conjugated to spmNPs by covalent binding of the antibody COOH groups to the NH_2 groups present onto the dextran coat of spmNPs so as to generate mAb198.3-spmNPs formulation potentially suitable for active and passive tumor targeting by applying external static magnetic field. Here we showed that, when conjugated to spmNPs, mAb198.3 maintained its ability to bind FAT1 on the surface of FAT1-positive colon cancer cell lines suggesting that the link with spmNPs did not affect mAb198.3 targeting on tumor cells. Moreover, despite the low mAb-loading capacity of spmNPs, the mAb198.3-spmNP formulation showed a high efficiency in reducing tumor growth *in vivo* using approximately 200 times lower doses compared to the free mAb198.3 indicating that this drug delivery system can improve mAb198.3 therapeutic activity at the site of action and therefore reduce its off-target cytotoxic effect. Further analysis should be performed to assess possible cytotoxicity that could derive from spmNPs accumulation *in vivo*.

To tackle this issue, a recently discovered erythrocyte-based platform, referred as Erythro-Magneto-HA-Virosome (EMHV) was used in this study. The EMHV simultaneously carried the spmNPs and mAb198.3 inside the erythrocytes and presented on its cytoplasmic membrane a fusogenic protein, the filamentous hemagglutinin (FHA), which facilitated the release of entrapped material (nanoparticles and drug) to the target area. We have previously shown that this novel DDS based on EMHV has the potential for magnetically-controlled site-specific anchoring, and highly efficient fusion capability with the targeted cells thus conferring an efficient drug release, directly inside target cells, together with magnetic NPs [23]. We have also shown that EMHV can increase the pharmacokinetics and pharmacodynamics as well as bioavailability of delivered drug at the site of action, thus reducing any systemic and off-target effects and consequently increasing the therapeutic efficacy and safety of treatments [16,18].

In this study, mAb198.3 was embedded within EMHVs generating a novel formulation for CRC treatment. The efficiency of EMHVs to homogeneously co-entrap mAb198.3 and spmNPs was demonstrated by Confocal Laser Scanning Microscopy, confirming that this erythrocyte-based DDS can efficiently deliver different class of therapeutic compounds including antibodies. In addition, the ability of the mAb198.3-EMHVs formulation to flow through the blood stream to the tumor area was shown through Power Doppler Mode imaging, demonstrating the efficiency of EMHV DDS in reaching the tumor area in a very short time. This is not surprising, since it is known that a massive angiogenic process from pre-existing vessels occurs during tumor mass formation to growth indefinitely [30]. Such hyper-vascularization and the high permeability of neo-blood vessels increase shedding of EMHVs into tumor mass, thus facilitating their subsequent accumulation in presence of a magnetic field. The IHC analysis, performed on tumor masses explanted from mAb198.3-EMHV-treated animals, further confirmed that the EMHV DDS localized in the cytoplasmatic membrane of tumor cells, indicating that EMHVs have reached the tumor mass and fused with the target cells. This EMHVs efficiency translated into a more efficient therapeutic action of the carried drug, as demonstrated by using animals treated with the mAb198.3-EMHVs formulation. mAb198.3-EMHV showed a higher anti-tumor activity, compared to the naked antibody, even if used at approximately 200 lower doses. In addition, the efficacy of this formulation was observed after fewer administration respect to the naked antibody, suggesting that the EMHVs increased not only the bioavailability but also the pharmacodynamics of the carried drug, even more efficiently than the mAb198.3-spmNP formulation. This was supported by the IHC analysis on *ex vivo* tumor specimens, which revealed a low staining grade of pro-proliferative K67 antigen in animals treated with mAb198.3 delivered with EMHV DDSs respect to the controls and to those treated with mAb198.3-spmNP.

While the therapeutic activity of mAb198.3–spmNP is likely due to FAT1 binding on the cell surface combined to receptor-antibody internalization, a well characterized property of mAb198.3[5–7], the anti-tumor activity of the mAb198.3–EMHVs formulation is somewhat surprising, since this DDS is expected to fuse with target cells and deliver the drug in the intracellular milieu. Although we cannot exclude that a small amount of mAb198.3 was released in the bloodstream by spontaneous lysis of some erythrocyte carries, most probably the largest antibody amount reached the intracellular compartment in target CRC cells and massively blocked FAT1 natural processing and/or recycling. Dedicated studies will be needed to investigate in depth the possible mAb198.3 intracellular mechanisms. Our IHC analysis evidenced a massive necrotic/apoptotic response in the group of animals treated with mAb198.3-EMHVs formulation respect to control and mAb198.3-spmNP groups, suggesting the involvement of apoptotic pathways.

Data so far generated suggest that the EMHV DDS is a powerful and flexible tool either for extra- or intracellular targets, able to drive antibodies as well as various pharmacologically active molecules into the tumor lesion. Importantly, as documented in our previous works, empty EMHVs are highly biocompatible and do not exert any immunological reaction or other detectable aspecific cytotoxic effect in vivo [16,18]. This is in line with the fact that red blood cells are innate biocompatible carriers and that spmNPs are already approved by FDA as contrast media for biomedical imaging (MNR) in the clinical practice, at significantly higher amount [31] than that entrapped into EMHVs.

In this study, an accurate a complete magnetic characterization for both DDS proposed was reported (for the first time, concerning EMHVs) and coupled with FEM simulations, demonstrating that an efficient anchoring in the tumor site is possible with a quite small magnetic field.

Our future investigations will be focused to test the proposed magnetically driven DDS for simultaneous delivery of multiple drugs having different mechanisms of actions and targeting different pathways. Such efforts are in accordance with the current common opinion that effective anti-cancer therapies should avail of the synergic action of multiple agents. Moreover, combination of conventional therapies, such as surgical resections, chemotherapy and radiotherapy, with targeted therapies, as anti-angiogenic immunotherapeutic agents, are likely to be the winning strategy [32]. On the other side, it is well known that any therapeutic approach may cause undesired side effects, which could be even exacerbated when used in combination. The innovative EMHV DDS described in this study could offer an interesting opportunity for multiple-agents therapies, being able to entrap different class of therapeutic compounds and to improve the pharmacokinetic activities of anti-cancer drugs with concomitant expected reduction of their intrinsic toxicity. EMHV DDS could offer also the ability to combine pharmacological therapy with therapeutic target thermal ablation, being an alternating magnetic field able to trigger the heating of magnetic nanoparticles carried by the DDS.

A final comment is related to future manufacturing and industrial development aspects. No major obstacles can be foreseen for spmNPs linked to antibodies, being these NPs already approved for human use. Concerning EMHV DDS, like other erythrocyte-based carriers, they are not suitable for long shelf-life storage; rather they must be rapidly administered to patients. The manufacturing of this type of product could be either centralized or bedside-based using dedicated medical devices, allowing the processing of autologous erythrocytes. Despite the undoubted challenges related to a future industrialization, including production scalability and quality control aspects, promising drug entrapment technologies based on osmotic methods used for erythrocyte-based delivery system preparation have been already industrialized and companies have already achieved many of the critical clinical stages [33]. In the next future, EMHVs carrying mAbs and other drugs could become a powerful and personalized tool to treat cancer and possibly other pathologies.

References

[1] J. Ferlay, D.M. Parkin, E. Steliarova-Foucher, Estimates of cancer incidence and mortality in Europe in 2008, Eur. J. Cancer. 46 (2010) 765–781. doi:10.1016/j.ejca.2009.12.014.

[2] J.B. O'Connell, M.A. Maggard, C.Y. Ko, Colon Cancer Survival Rates With the New American Joint Committee on Cancer Sixth Edition Staging, JNCI J. Natl. Cancer Inst. 96 (2004) 1420–1425. doi:10.1093/jnci/djh275.

[3] F. Ciardiello, N. Kim, T. Saeki, R. Dono, M.G. Persico, G.D. Plowman, J. Garrigues, S. Radke, G.J. Todaro, D.S. Salomon, Differential expression of epidermal growth factor-related proteins in human colorectal tumors., Proc. Natl. Acad. Sci. U. S. A. 88 (1991) 7792–6. http://www.ncbi.nlm.nih.gov/pubmed/1715580 (accessed September 26, 2017).

[4] S. Hagan, M.C.M. Orr, B. Doyle, Targeted therapies in colorectal cancer—an integrative view by PPPM, EPMA J. 4 (2013) 3. doi:10.1186/1878-5085-4-3.

[5] P. Pileri, S. Campagnoli, A. Grandi, M. Parri, E. De Camilli, C. Song, L. Ganfini, A. Lacombe, I. Naldi, P. Sarmientos, C. Cinti, B. Jin, G. Grandi, G. Viale, L. Terracciano, R. Grifantini, FAT1: a potential target for monoclonal antibody therapy in colon cancer, Br. J. Cancer. 115 (2016) 40–51. doi:10.1038/bjc.2016.145.

[6] L. Fan, S. Campagnoli, H. Wu, A. Grandi, M. Parri, E. De Camilli, G. Grandi, G. Viale, P. Pileri, R. Grifantini, C. Song, B. Jin, Negatively charged AuNP modified with monoclonal antibody against novel tumor antigen FAT1 for tumor targeting., J. Exp. Clin. Cancer Res. 34 (2015) 103. doi:10.1186/s13046-015-0214-x.

[7] L. Fan, Y. Zhang, F. Wang, Q. Yang, J. Tan, R. Grifantini, H. Wu, C. Song, B. Jin, Multifunctional all-in-one drug delivery systems for tumor targeting and sequential release of three different anti-tumor drugs, Biomaterials. 76 (2016) 399–407. doi:10.1016/j.biomaterials.2015.10.069.

[8] N. Lee, T. Hyeon, Designed synthesis of uniformly sized iron oxide nanoparticles for efficient magnetic resonance imaging contrast agents, Chem. Soc. Rev. 41 (2012) 2575–2589. doi:10.1039/C1CS15248C.

[9] E. Cheraghipour, S. Javadpour, A.R. Mehdizadeh, Citrate capped superparamagnetic iron oxide nanoparticles used for hyperthermia therapy, J. Biomed. Sci. Eng. 5 (2012) 715–719. doi:10.4236/jbise.2012.512089.

[10] R. Tietze, J. Zaloga, H. Unterweger, S. Lyer, R.P. Friedrich, C. Janko, M. Pöttler, S. Dürr, C. Alexiou, Magnetic nanoparticle-based drug delivery for cancer therapy, Biochem. Biophys. Res. Commun. 468 (2015) 463–470. doi:10.1016/j.bbrc.2015.08.022.

[11] M. De Simone, D. Panetta, E. Bramanti, C. Giordano, M.C. Salvatici, L. Gherardini, A.

Menciassi, S. Burchielli, C. Cinti, P.A. Salvadori, Magnetically driven nanoparticles: ^{18} FDG-radiolabelling and positron emission tomography biodistribution study, Contrast Media Mol. Imaging. 11 (2016) 561–571. doi:10.1002/cmmi.1718.

[12] T.M. Allen, P.R. Cullis, Drug Delivery Systems: Entering the Mainstream, Science (80-.). 303 (2004) 1818–1822. doi:10.1126/science.1095833.

[13] R.K. Chowdhary, I. Shariff, D. Dolphin, Drug release characteristics of lipid based benzoporphyrin derivative., J. Pharm. Pharm. Sci. 6 (n.d.) 13–9. http://www.ncbi.nlm.nih.gov/pubmed/12753726 (accessed September 26, 2017).

[14] J.C. Roth, D.T. Curiel, L. Pereboeva, Cell vehicle targeting strategies, Gene Ther. 15 (2008) 716–729. doi:10.1038/gt.2008.38.

[15] M. Hamidi, A. Zarrin, M. Foroozesh, S. Mohammadi-Samani, Applications of carrier erythrocytes in delivery of biopharmaceuticals, J. Control. Release. 118 (2007) 145–160. doi:10.1016/j.jconrel.2006.06.032.

[16] M.Taranta. I. Naldi, S.Grimaldi, L. Salvini, PP. Claudio, F.Rocchio, AF.Munoz, S.Prete, C. Cinti, Magnetically Driven Bio reactors as new Tools in Drug Delivery, J. Bioanal. Biomed. s5 (2011). doi:10.4172/1948-593X.S5-002.

[17] H. Lewis, David A; OyaAlpar, Therapeutic possibilities of drugs encapsulated in erythrocytes, Int. J. Pharm. 22 (1984) 137–146. doi:10.1016/0378-5173(84)90017-6.

[18] I. Naldi, M. Taranta, L. Gherardini, G. Pelosi, F. Viglione, S. Grimaldi, L. Pani, C. Cinti, Novel epigenetic target therapy for prostate cancer: a preclinical study., PLoS One. 9 (2014) e98101. doi:10.1371/journal.pone.0098101.

[19] C. Song, B. Yan, L. Chen, Y. Li, Y. Wei, Y. Sun, A. Yang, K. Yang, B. Jin, Novel Immunohistochemical Monoclonal Antibody Against Rat B Cell Receptor Associated Protein 31 (BAP31), Hybridoma. 28 (2009) 363–367. doi:10.1089/hyb.2009.0027.

[20] M. Parri, L. Pietrovito, A. Grandi, S. Campagnoli, E. De Camilli, F. Bianchini, S. Marchiò, F. Bussolino, B. Jin, P. Sarmientos, G. Grandi, G. Viale, P. Pileri, P. Chiarugi, R. Grifantini, Angiopoietin-like 7, a novel pro-angiogenetic factor over-expressed in cancer, Angiogenesis. 17 (2014) 881–896. doi:10.1007/s10456-014-9435-4.

[21] E.P. Furlani, K.C. Ng, Analytical model of magnetic nanoparticle transport and capture in the microvasculature., Phys. Rev. E. Stat. Nonlin. Soft Matter Phys. 73 (2006) 61919. doi:10.1103/PhysRevE.73.061919.

[22] D.J. Langford, A.L. Bailey, M.L. Chanda, S.E. Clarke, T.E. Drummond, S. Echols, S. Glick, J. Ingrao, T. Klassen-Ross, M.L. Lacroix-Fralish, L. Matsumiya, R.E. Sorge, S.G. Sotocinal, J.M. Tabaka, D. Wong, A.M.J.M. van den Maagdenberg, M.D. Ferrari, K.D. Craig, J.S.

Mogil, Coding of facial expressions of pain in the laboratory mouse., Nat. Methods. 7 (2010) 447–9. doi:10.1038/nmeth.1455.

[23] C. Cinti, M. Taranta, I. Naldi, S. Grimaldi, Newly engineered magnetic erythrocytes for sustained and targeted delivery of anti-cancer therapeutic compounds., PLoS One. 6 (2011) e17132. doi:10.1371/journal.pone.0017132.

[24] A.M.J. Davis, K.B. Ranger, A STOKES FLOW MODEL FOR THE DRAG ON A BLOOD CELL*, (1987) 305–311. http://www.ams.org/journals/qam/1987-45-02/S0033-569X-1987-0895100-X/S0033-569X-1987-0895100-X.pdf (accessed October 19, 2017).

[25] M.A. Postow, M.K. Callahan, J.D. Wolchok, Immune Checkpoint Blockade in Cancer Therapy, J. Clin. Oncol. 33 (2015) 1974–1982. doi:10.1200/JCO.2014.59.4358.

[26] S.L. Topalian, C.G. Drake, D.M. Pardoll, Immune Checkpoint Blockade: A Common Denominator Approach to Cancer Therapy, Cancer Cell. 27 (2015) 450–461. doi:10.1016/j.ccell.2015.03.001.

[27] P. Boland, W. Ma, Immunotherapy for Colorectal Cancer, Cancers (Basel). 9 (2017) 50. doi:10.3390/cancers9050050.

[28] W. Cai, X. Chen, Nanoplatforms for targeted molecular imaging in living subjects., Small. 3 (2007) 1840–54. doi:10.1002/smll.200700351.

[29] C.J. Murphy, A.M. Gole, J.W. Stone, P.N. Sisco, A.M. Alkilany, E.C. Goldsmith, S.C. Baxter, Gold Nanoparticles in Biology: Beyond Toxicity to Cellular Imaging, Acc. Chem. Res. 41 (2008) 1721–1730. doi:10.1021/ar800035u.

[30] A. Maiorana, P.M. Gullino, Acquisition of angiogenic capacity and neoplastic transformation in the rat mammary gland., Cancer Res. 38 (1978) 4409–14. http://www.ncbi.nlm.nih.gov/pubmed/102422 (accessed September 27, 2017).

[31] H.P. Niendorf, M. Laniado, W. Semmler, W. Schörner, R. Felix, Dose administration of gadolinium-DTPA in MR imaging of intracranial tumors., AJNR. Am. J. Neuroradiol. 8 (n.d.) 803–15. http://www.ncbi.nlm.nih.gov/pubmed/2823588 (accessed September 27, 2017).

[32] I. Melero, D.M. Berman, M.A. Aznar, A.J. Korman, J.L. Pérez Gracia, J. Haanen, Evolving synergistic combinations of targeted immunotherapies to combat cancer., Nat. Rev. Cancer. 15 (2015) 457–72. doi:10.1038/nrc3973.

[33] V. Bourgeaux, J.M. Lanao, B.E. Bax, Y. Godfrin, Drug-loaded erythrocytes: on the road toward marketing approval., Drug Des. Devel. Ther. 10 (2016) 665–76. doi:10.2147/DDDT.S96470.

ACKNOWLEGMENTS
This work has been supported by Regione Toscana and European funds with the POR-CREO-FESR 2007/2013 ACTILA project, the national flagship project NANOMAX funds with the ENCODER project and by CNR funds.
The authors thanks Dr. BOQUAN JIN, of the Fourth Military Medical University, Xi'an, China for mAb198.3 hybridoma manufacturing.
S.T wishes to thank the national flagship project NANOMAX for the funding with the project ENCODER. M.T wishes to thank the Regione Toscana for funding POR-CREO-FESR 2007/2013 ACTILA project.